Atmospheric Environment 147 (2016) 224–233

Contents lists available at ScienceDirect

Atmospheric Environment

journal homepage: www.elsevier.com/locate/atmosenv

Impact of aerosol hygroscopic growth on the direct aerosol radiative effect in summer on North China Plain

Y. Kuang [a], C.S. Zhao [a, *], J.C. Tao [a], Y.X. Bian [a], N. Ma [b]

[a] Department of Atmospheric and Oceanic Sciences, School of Physics, Peking University, Beijing, China
[b] Leibniz Institute for Tropospheric Research, Leipzig, Germany

HIGHLIGHTS

- High frequency of high RH (>80%) profiles within the mixed layer during daytime.
- Aerosol optical properties highly depend on RH profiles due to aerosol water uptake.
- Aerosol hygroscopicity contributes to direct aerosol radiative effect significantly.

ARTICLE INFO

Article history:
Received 8 April 2016
Received in revised form
3 October 2016
Accepted 7 October 2016
Available online 8 October 2016

Keywords:
Relative humidity profiles
Aerosol optical depth
Single scattering albedo
Asymmetry factor
Aerosol optical properties

ABSTRACT

In this paper, relative humidity (RH) profiles and their impacts on the vertical variations of aerosol optical properties and the direct aerosol radiative effect (DARE) have been investigated based on surface measurements from the Haze in China campaign and sounding data from the North China Plain. Among the profiles obtained from July to September in 2008, about half have RHs greater than 80% within the mixed layer. The vertical variations in the aerosol optical properties at ambient RH, including the extinction coefficient (σ_{ext}), single scattering albedo (SSA) and asymmetry factor (g), are remarkably different from the variations in the dry aerosols and are highly dependent on the RH profiles. Increases of the aerosol optical depth and column-averaged SSA and g due to aerosol water uptake can reach up to 64%, 0.052 and 0.079, respectively. The fractional contribution to the instantaneous DARE at the top of the atmosphere due to aerosol hygroscopic growth reaches 60% in high RH profiles. DARE estimates can be significantly biased if the RH dependence of SSA or g is not considered. We suggest that if their vertical profiles or column-averaged values are absent, then the ambient values of SSA and g at the surface should be used rather than the values of SSA and g obtained from dry aerosols when estimating DAREs.

1. Introduction

Tropospheric aerosols affect the energy balance on the Earth by directly scattering and absorbing solar radiation and indirectly changing the properties and lifespans of clouds (Boucher et al., 2013). The changes in irradiance due to the interaction of aerosol and radiation are commonly described in terms of the direct aerosol radiative effect (DARE), and their estimates remain largely uncertain (Boucher et al., 2013). These uncertainties are mainly caused by the high temporal, spatial and compositional variability of aerosols as well as RH fields and an incomplete understanding of related, integral aerosol optical properties.

Because many components of aerosol particles are hygroscopic, the particles can take up water and change in size depending on their chemical composition and the ambient relative humidity (RH). Hygroscopic growth becomes particularly important when the RH is greater than 60% and water often comprises more than 50% of the fine particle mass when the RH exceeds 70–80% (Bian et al., 2014; McMurry, 2000). Therefore, RH is an important parameter that governs the optical properties of aerosols and DARE. Previously, numerous studies have investigated the dependence of aerosol optical properties on RH by considering the aerosol scattering coefficient (σ_{sp}) (Zieger et al., 2013), single scattering albedo (SSA) (Tao et al., 2014; Yoon and Kim, 2006), hemispheric scattering coefficient (Titos et al., 2014) and asymmetry factor (g) (Yoon and Kim, 2006). However, these studies were mainly based on surface measurements and only considered the RH at the surface.

Few studies have investigated the influence of RH profiles on the

* Corresponding author.
E-mail address: zcs@pku.edu.cn (C.S. Zhao).

http://dx.doi.org/10.1016/j.atmosenv.2016.10.013
1352-2310/

columnar aerosol optical properties generally used to estimate the DARE at the top of the atmosphere (TOA) and at the surface. Using meteorological and aerosol measurements obtained aboard an aircraft, Yoon and Kim (2006) presented RH and σ_{sp} profiles under ambient and low RH conditions and demonstrated that σ_{sp} is significantly enhanced at ambient RH conditions relative to dry conditions. However, in that study, the vertical characteristics of RH and the influences of RH profiles on the aerosol optical depth (AOD), column-averaged SSA and g were not analyzed. Using RH measurements and a system of two nephelometers operated in parallel aboard an aircraft, Shinozuka et al. (2007) investigated the influences of RH profiles on ambient AOD and found that the fraction of ambient AOD due to water uptake was 37 ± 15% (average and standard deviation). Observationally based sensitivity studies conducted by Brock et al. (2016) indicate that the relationship between AOD and dry aerosol mass can be highly variable but is especially sensitive to RH. However, the influences of the RH profiles on SSA and g were not investigated.

A few researchers have studied the influence of RH on estimates of DARE. The results of Hignett et al. (1999) revealed that at a RH of 80% the DARE at the TOA was roughly twice that of the dry aerosols. Im et al. (2001) found that the average ratios between the DARE at the TOA when the RH was 80% and 30% were nearly constant at 1.45 ± 0.01 for three different types of air masses, including polluted continental air, marine air and continental air. Several other studies bases on field measurements also investigated the influence of RH on DARE by assuming that the RH was constant across the aerosol layer (Yoon and Kim, 2006).

In summary, the real influence of variation of RH in the vertical on the local and column integral optical properties of aerosols and the DARE are not well understood. The cooling effect of atmospheric aerosols is amplified by their hygroscopic growth and the degree of amplification varies in time and space (Cheng et al., 2008; Yoon and Kim, 2006). For some areas where highly absorbing aerosols prevail, the hygroscopic behavior of aerosols will largely enhance the light scattering abilities of the aerosols and may result in the transition of the DARE from warming to cooling at the TOA (Cheng et al., 2008; Titos et al., 2014), which is very important when studying the regional climate effects induced by anthropogenic aerosols. Therefore, the effects of RH profiles on the vertical structures of aerosol optical properties should be addressed to better understand the influences of RH profiles on AOD, column-averaged SSA, g and estimates of DARE.

In this study, the vertical RH characteristics are addressed, and several typical types of RH profiles are described based on radiosonde measurements taken in Beijing in 2008. Based on aerosol observations from a representative background site on the North China Plain (NCP) and the aforementioned typical RH profiles, a numerical study was conducted to investigate the influences of RH profiles on the vertical structures of aerosol optical properties and DARE at the TOA and at the surface.

The vertical profile measurements of RH and other relevant parameters and the corresponding analytical methods are briefly described in Sect. 2.1. The aerosol optical properties throughout the profile were calculated using Mie theory, and the corresponding assumptions are described and discussed in Sect. 2.2. The radiative transfer calculation is presented in Sect. 2.3. The results of the study and discussions are presented in Sect. 3, and the conclusions of the study are presented in Sect. 4.

2. Data and methods

2.1. Vertical RH profiles

The profiles of the meteorological parameters (including atmospheric pressure, temperature, RH, wind speed and wind direction) were observed intensively using a GTS1 (Bian et al., 2011) digital radiosonde from July to September in 2008 at the meteorological bureau of Beijing (39°48′N, 116°28′E). The elevation of this site is 33 m, and the obtained profiles have a vertical resolution of 10 m. During this intensive observation period, balloon soundings were performed four times per day at the local times of 01:30, 07:30, 13:30 and 19:30. Because direct interactions between aerosols and solar shortwave radiation only occur during the daytime, only the profiles obtained at the local time of 13:30 were used to analyze the vertical characteristics of RH. In total, 81 profiles are available.

At the local time of 13:30, especially in the summer, due to extensive turbulent mixing, the concentrations of water vapor and other pollutants remain reasonably steady within the layer whose vertical thickness is referred to as the mixed layer height (MH). In this study, only profiles that exhibit well-mixed vertical structures are considered when analyzing the vertical characteristics of RH. Similar to the method described by Srivastava et al. (2010), the virtual potential temperature (θ_v) and specific humidity (q) were used together to quantitatively estimate the MH. In addition, the top of the mixed layer was identified as the height at which the first significant inversions in the θ_v and q profiles are evident. With the parameters of the observed profiles, θ_v and q can be calculated using the following equations:

$$\theta_v = \theta(1 + 0.61\mathrm{r}) \tag{1}$$

$$\mathrm{q} = 0.623e/(p - 0.377e) \tag{2}$$

where θ is the potential temperature (K), r is the mixing ratio (kg/kg) of water vapor, p is the ambient pressure (mbar), and e is water vapor pressure (mbar) of the air parcel.

Based on this method for estimating MH, 56 profiles (approximately 70% of all the profiles) exhibited distinct boundary layer mixing structures. The MH values of these 56 profiles were determined. To investigate the vertical structures of RH and other parameters, the evolution of the MH should be considered statistically. According to the method described by Ferrero et al. (2014), vertical profiles with different MH values can be averaged by considering the position of each measured data point relative to the MH. Thus, the vertical profiles were first normalized by introducing a standardized height (H_s), which was calculated as follows:

$$H_s = \frac{z - MH}{MH} \tag{3}$$

where z is the height above the ground and H_s is 0 at the MH and −1 at ground level. Then, the vertical profiles were averaged to understand the vertical structures of the corresponding parameters.

2.2. Aerosol optical property calculations and corresponding assumptions

To calculate σ_{ext}, SSA and g of the aerosol particles along the vertical profiles using the Mie code (Bohren and Huffman, 2008), data on the vertical aerosol particle number size distribution (PNSD), chemical composition, hygroscopicity, mixing state and RH are needed. Four types of RH profiles corresponding to different degrees of humidity were used to calculate σ_{ext}, SSA and g. During the first period of the Haze in China (HaChi) campaign (from July 12 to August 14 in 2009), the optical, chemical, and hygroscopic properties and the size distributions of the aerosols were observed at the Wuqing meteorological station. Wuqing is located in the

heart of the plain region, and the distance between Wuqing and downtown Beijing is approximately 80 km. Wuqing is highly representative of the polluted NCP region (Xu et al., 2011). Thus, the vertical PNSD, aerosol hygroscopicity, mass concentration and mixing state of black carbon (BC) used in this study were assumed based on surface measurements from the HaChi campaign (Ma et al., 2012a) or by a type of parameterization scheme. The corresponding assumptions and parameterization schemes are described and discussed below.

Liu et al. (2009) observed the vertical distributions of aerosols by conducting an aircraft study over Beijing where RH profile observations were conducted. Their results demonstrated that the aerosol particle number concentration (N_a) was relatively uniform within the mixed layer and declined rapidly above the inversion layer. A parameterization scheme was provided in their research and has been adopted in this study to describe the vertical variations in N_a. This scheme requires three parameters termed H_{PBL}, H_{LD} and N_0. H_{PBL} is the height of the planetary boundary layer and is determined from the gradient of N_a. The results of Ferrero et al. (2014) indicated that the MH or H_{PBL} retrieved from the profiles of N_a, temperature and RH agree very well with each other. Thus, the MH retrieved from the profiles of θ_v and q in this study was substituted for H_{PBL} needed in the scheme. H_{LD} is the thickness of a transition layer known as the linear decrease layer and was reported to be equal to 200 m by Liu et al. (2009). Because the MH retrieved in this study mainly varied from 700 m to 2000 m (see Sect. 3.1), which is similar to the range of H_{PBL} in Liu et al. (2009), the H_{LD} in this research was also set to 200 m. N_0 is the value of N_a at the surface and in this study is set to 12,500 cm^{-3}, which is the average value of N_a at the local time of 13:30 measured during the HaChi campaign. During the HaChi campaign, the PNSD at dry state ranging from 3 nm to 10 μm was observed jointly by an Aerodynamic Particle Sizer (APS, TSI Inc., Model 3321) and a Twin Differential Mobility Particle Sizer (TDMPS, Leibniz-Institute for Tropospheric Research (IfT), Germany; Birmili et al. (1999)) with a temporal resolution of 10 min, and N_a can be calculated through measured PNSD. The normalized PNSD (nPNSD) is defined using the following equation:

$$f(\log D_i) = \frac{N_i/\Delta\log D_i}{\sum_i N_i} = \frac{N_i/\Delta\log D_i}{N_a} \quad (4)$$

where D_i (nm) is the diameter of the aerosol particle in the i^{th} bin, N_i is the particle number concentrations in the i^{th} bin, and $\Delta\log D_i = \log D_i^{upper} - \log D_i^{lower}$, where D_i^{upper} and D_i^{lower} refer to the upper and lower bounds of the i^{th} bin, respectively. The results of Liu et al. (2009) indicated that the nPNSD at dry state in the profiles during periods of no dust have similar shapes at different altitudes. In addition, the results of Ferrero et al. (2010) indicated that the mean diameter and volume concentrations of fine particles vary little within the well mixed boundary layer. Therefore, it was assumed that the nPNSD at dry state does not vary with height; thus, the average nPNSD at dry state from the HaChi campaign at the local time of 13:30 was used.

Although several BC measurements have been reported over regions in Asia and Europe and over some oceans, BC profiles are globally scarce compared with ground-level data (Ferrero et al., 2014). The observational constraints on the vertical distribution of BC are poor, particularly in the NCP. Consequently, no available parameterization schemes for the vertical distribution of BC exist. However, the results of Ferrero et al. (2011) indicated that the total number of aerosol particles and the mass concentration of BC (M_{BC}) were impacted in the same way by vertical mixing and that most BC lies within the MH. In addition, the M_{BC} was often observed to behave similarly to N_a with altitude (Ferrero et al., 2011; 2014). Furthermore, the refractory BC concentrations remained relatively constant throughout the mixed layer in all of the profiles presented by McMeeking et al. (2011). Recently, results of Ran et al. (2016) demonstrated that concentrations of BC remained relatively constant throughout the mixed layer and decreased significantly above the mixed layer during summer on the NCP. Hence, in this research, M_{BC} was assumed to be constant within the MH and to decrease with altitude in the same way as the vertical parameterization scheme used for N_a. To achieve this, the ratio between M_{BC} and N_a was assumed to be constant in the vertical direction, that is, $M_{BC}(z) = N_a(z) \times M_{BC}(surface)/N_0$, where $M_{BC}(z)/M_{BC}(surface)$ and $N_a(z)/N_0$ are M_{BC} and N_a at altitude z/surface. The M_{BC} at the surface was obtained from surface measurements during the HaChi campaign, and the average M_{BC} at the local time of 13:30 (i.e., 4752 ng/m^3) was used. During the HaChi campaign, the absorption coefficient at 637 nm was measured using a Multi-angle Absorption Photometer (MAAP Model 5012, Thermo, Inc., Waltham, MA USA) with a temporal resolution of 1 min, and further transformed into black carbon (BC) mass concentrations with a constant mass absorption efficiency (MAE) of 6.6 $m^2\ g^{-1}$.

Regarding the mixing state of BC with height, few studies have reported the aging of BC along vertical profiles (McMeeking et al., 2011; Moteki et al., 2007). Particularly in the NCP, no observations have been reported regarding the vertical evolution of the mixing state of BC. The results of McMeeking et al. (2011) showed that the number fraction of "thickly coated" refractory BC particles remains nearly constant within the boundary layer and then increases above the boundary layer. Therefore, the BC mixing state varies little within the mixed layer under well-mixed conditions and as a result of aging processes becomes more internal above the MH. Additionally, in terms of the parameterization scheme of N_a used in this paper, the aerosol particles are mainly located within the mixed layer. Therefore, we assumed that the mixing state of BC did not vary with height in this study. The results of Ma et al. (2012a) demonstrated that, during the HaChi campaign period, it is appropriate to assume that both externally mixed and core-shell mixed BC particles exist and to perform aerosol optical calculations accordingly. The mixing state of BC for ambient aerosols is described by the ratio between the mass of the externally mixed BC and the total BC as follows:

$$r_{ext-BC} = \frac{M_{ext-BC}}{M_{BC}} \quad (5)$$

where M_{ext-BC} is the mass concentration of the externally mixed BC and M_{BC} is the total mass concentration of BC. A high-resolution time series of r_{ext-BC} was also provided in Ma et al. (2012a), and its average at the local time of 13:30 (a value of 0.45) was used as the mixing state of BC in this study, and this ratio remains constant at different altitudes. The mass size distribution of BC used to retrieve the mixing state in Ma et al. (2012a) was also used in this research.

With regard to aerosol hygroscopicity. The average size-resolved hygroscopicity parameter κ (Petters and Kreidenweis, 2007) introduced in Chen et al. (2012) is used to account for aerosol hygroscopic growth in this study. Hygroscopic parameter κ in research of Chen et al. (2012) was derived from the ground measurements of aerosol hygroscopic growth factor during the HaChi campaign and aerosol hygroscopic growth factor is obtained using a High Humidity Tandem Differential Mobility Analyzer. Furthermore, due to above assumptions associated with aerosol properties are based on the boundary layer is well mixed, thus, the used size-resolved κ is also assumed constant at different altitudes.

By combining the vertical information of the PNSD, the mass concentration and mixing state of BC, the aerosol particle

hygroscopicity, and the RH profiles introduced above, the vertical profiles of the aerosol optical properties can be calculated using Mie theory. Details regarding these calculations can be found in Kuang et al. (2015).

The AOD at 550 nm was calculated by using the following formula:

$$\mathrm{AOD} = \int_0^{10km} \sigma_{ext}(z)dz \tag{6}$$

where $\sigma_{ext}(z)$ is the extinction coefficient at 550 nm at altitude z.

SSA and g are usually held constant with altitude when estimating the DARE (Myhre, 2009). In addition, the column-averaged values of SSA and g retrieved from ground-based sun-sky radiometers are widely used, although they both have distinct vertical structures. For every profile, the column-averaged SSA was calculated using the following formula (Schafer et al., 2014):

$$SSA_{column-averaged} = \frac{\int_0^{10km} \sigma_{ext}(z) \times SSA(z)dz}{AOD} \tag{7}$$

where $\sigma_{ext}(z)$ and $SSA(z)$ are the extinction coefficient and SSA at an altitude of z, respectively, and the column-averaged value of g was calculated in the same way.

2.3. Estimating the DARE

Aerosol scattering and absorption of solar radiation can modify the energy balance of Earth-atmosphere systems. The DARE can be estimated using radiative transfer model (RTM) simulations. In this study, the Santa Barbara DISORT (discrete ordinates radiative transfer) Atmospheric Radiative Transfer (SBDART) model (Ricchiazzi et al., 1998) is used to estimate the DARE, and RTM simulations are performed for cloud-free conditions.

The instantaneous DARE was quantified either at the TOA or at the surface as the change in the net radiative flux between atmospheric conditions with and without the aerosols in the atmosphere as follows:

$$\mathrm{F} = (f_a\downarrow - f_a\uparrow) - (f_0\downarrow - f_0\uparrow) \tag{8}$$

where F is the DARE; f denotes the downward/upward irradiance, which spans the wavelength range of 0.25–4 μm; and $(f\downarrow - f\uparrow)$ denotes the net irradiance computed with a given aerosol, f_a, or without aerosols, f_0, at the TOA or surface.

In this study, because the RH profiles observed at the local time of 13:30 are used, only the instantaneous DARE at this time is evaluated. Three types of inputs are used in the SBDART simulations: (1) the aerosol optical properties in vertical profiles, (2) the atmospheric gas and meteorological parameter profiles, and (3) the surface albedo. The vertical profiles of the aerosol optical properties included the profiles of σ_{ext}, SSA and g were calculated at four wavelengths (470 nm, 550 nm, 860 nm and 1240 nm) with a height resolution of 50 m. The required vertical profiles of water vapor, pressure and temperature are obtained from radiosonde observations. The vertical contents of other atmospheric gases provided by SBDART are used in the simulations. The surface albedo values used in the simulations are obtained from the Moderate Resolution Imaging Spectroradiometer (MODIS) V005 climate modeling grid (CMG) Albedo Product (MCD43C3) from August 1, 2009 at Wuqing, where the HaChi campaign was conducted.

3. Results and discussion

From the RH profiles observed in Beijing, the vertical structures of the RH profiles in the NCP are characterized. The roles of the RH profiles in the vertical structures of the aerosol optical properties and the estimation of DARE are carefully analyzed.

3.1. The vertical characteristics of RH

One radiosonde profile was available per day at the local time of 13:30 from July to September, resulting in 81 available profiles. Among these profiles, 56 (approximately 70%) have a distinct mixed layer structure. The vertical profiles of q, temperature and RH were normalized using the methods introduced in Sect. 2.1 and are shown in Fig. 1. The q values were generally uniform within the mixed layer, with an average of 10 g/kg at the surface, indicating that the water vapor content is well mixed due to the strong turbulence in the mixed layer. The water vapor concentration decreased sharply above the MH. The temperature profiles are shown in Fig. 1. The average vertical temperature profile clearly indicates that an elevated inversion layer exists at the top of the MH, which limits the vertical diffusion of water vapor from the mixed layer to the free troposphere. The average RH profile demonstrates that the RH at the surface (SRH) is relatively low (approximately 40%) and increases with altitude in the mixed layer.

The MH retrieved from all well-mixed profiles is shown in Fig. 2 and mainly ranges from 700 m to 2000 m, with an average value of approximately 1500 m. The maximum RH within the mixed layer, which is referred to as MRH hereafter, is not obviously correlated with the MH. The frequency distribution of MRH is analyzed to better understand the distribution of humidity in the profiles, as shown in Fig. 3. More than 80% of the investigated profiles have MRHs greater than 60%, and approximately 52% of the investigated profiles have MRHs greater than 80%. The profiles with MRHs ranging from 80% to 90% account for the largest percentage (approximately 34%) of the profiles, and profiles with MRHs ranging from 90% to 100% account for the second largest percentage. In contrast, the SRH mainly ranges from 30% to 60%, which implies that high RH profiles prevail during the summer on the NCP, even when the RH at the surface is relatively low.

To analyze the vertical characteristics of the profiles with different levels of RH profiles, the profiles are classified into four groups (1–4) consisting of the following MRH ranges: 60%–70%, 70%–80%, 80%–90% and 90%–95%. Here, we define profiles with MRHs greater than 80% as highly humid profiles (groups 3 and 4) and profiles with MRHs greater than 60% but less than 80% as humid profiles (groups 1 and 2). The average vertical q and RH structures of the four groups are shown in Fig. 4. The q values of the highly humid groups are obviously greater than those of the humid groups, but these values differ very little within the highly humid and humid groups. Within the same group, the RH has a similar vertical shape within the MH. Nevertheless, significant differences are present in the free troposphere. The average SRHs (and the difference between the MRH and the SRH) for groups 1 through 4 are 37.1% (25.7%), 38.1% (32.1%), 48.8% (33.4%) and 54.1% (36.3%), respectively. Similar to the q values, the SRH differs greatly between highly humid and humid groups but differs little within the peer groups. Generally, the difference between the MRH and the SRH increases as the MRH increases.

3.2. The roles of RH profiles in the vertical structures of aerosol optical properties

Four groups of RH profiles are detailed in Sect. 3.1 based on their MRH ranges, and their corresponding average profiles representing

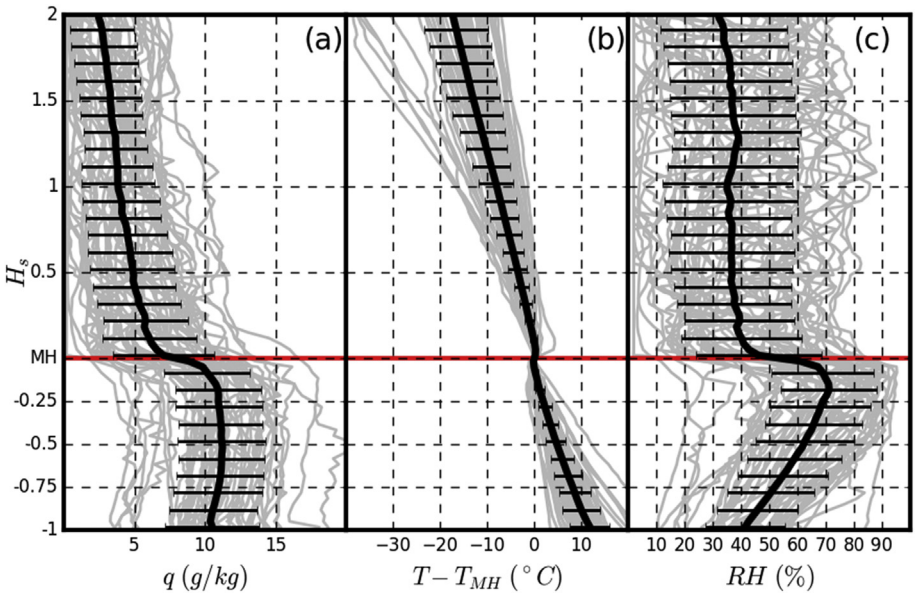

Fig. 1. The vertical structures of (a) q, (b) temperature minus the temperature at the MH, and (c) RH. The red line marks the position of the MH, the solid black lines represent the average profile of corresponding profiles, and the bars represent the standard deviations. (For interpretation of the references to colour in this figure legend, the reader is referred to the web version of this article.)

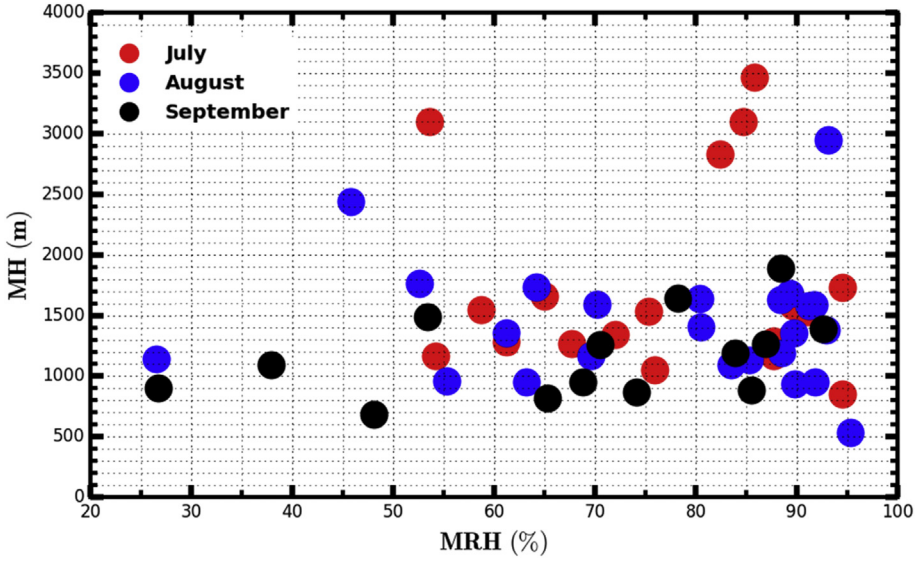

Fig. 2. The distribution of MH; the x axis represents the MRH of the profiles.

different levels of RH were used to determine the influences of RH profiles on aerosol optical properties. The methods used to calculate aerosol optical properties and the required assumptions are discussed in Sect. 2.2. The average RH profiles of groups 1 to 4 are referred as P60–70, P70–80, P80–90 and P90–95, and their MRH values are 62.8%, 70.1%, 82.1% and 90.4%, respectively. The MH was set as 1500 m, which is the average of the MH values retrieved from all well-mixed profiles. The calculated vertical structures of σ_{ext}, SSA and g at 550 nm under dry and ambient conditions for the four group-average RH profiles are shown in Fig. 5. Under dry conditions and based on the assumptions introduced before, the value of σ_{ext} was held constant within the MH and began to decrease dramatically above the MH. At the surface, the σ_{ext} at 550 nm is 343.4 Mm^{-1}. The SSA and g under dry conditions remained constant with altitude because it was assumed that the mixing state of BC and the ratio between M_{BC} and N_a do not vary with altitude, and corresponding values of SSA and g at 550 nm are 0.87 and 0.63, respectively. The profiles of σ_{ext}, SSA and g corresponding to the four group-averaged RH profiles were remarkably different from the profiles of the dry state aerosols and were highly dependent on the RH profiles. Within the mixed layer, the σ_{ext}, SSA and g of the ambient aerosols were lowest at the surface and gradually increased to maximum values near the top of the mixed layer. The differences between the maximum and minimum σ_{ext}/SSA/g at 550 nm within the MH for P60–70, P70–80, P80–90 and P90–95 were 71.4/0.019/0.030, 115.1/0.027/0.042, 242.2/0.041/0.061 and 539.6/0.059/0.088, respectively (σ_{ext} is presented in units of Mm^{-1}). These results demonstrate that although the RH is relatively low at the surface, the aerosol optical properties become more sensitive to RH as the RH increases. Thus, the change in RH with altitude

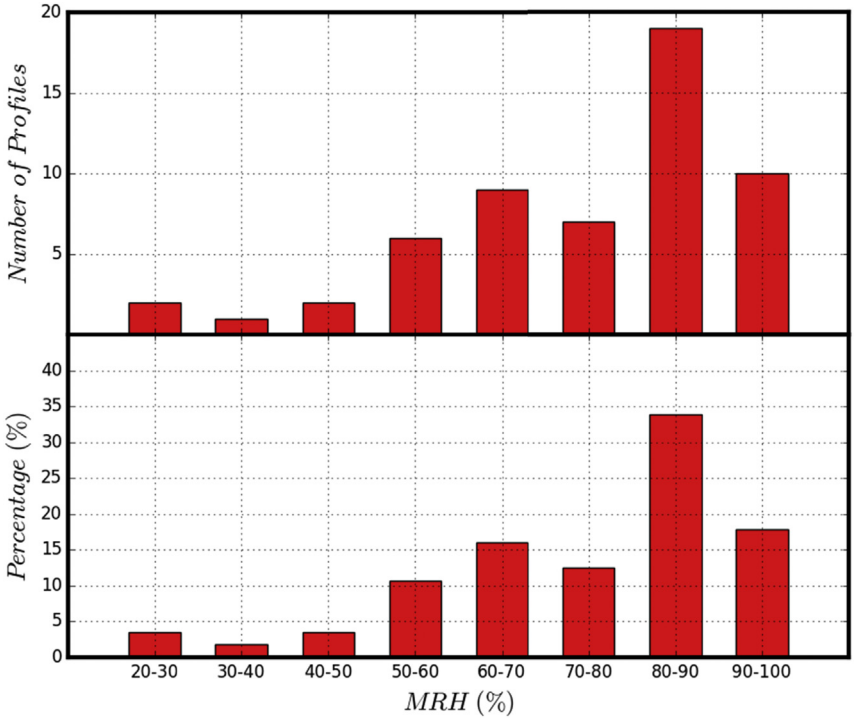

Fig. 3. The frequency distribution of the MRH. This result indicates that high RH profiles are prevalent during the summer on the NCP.

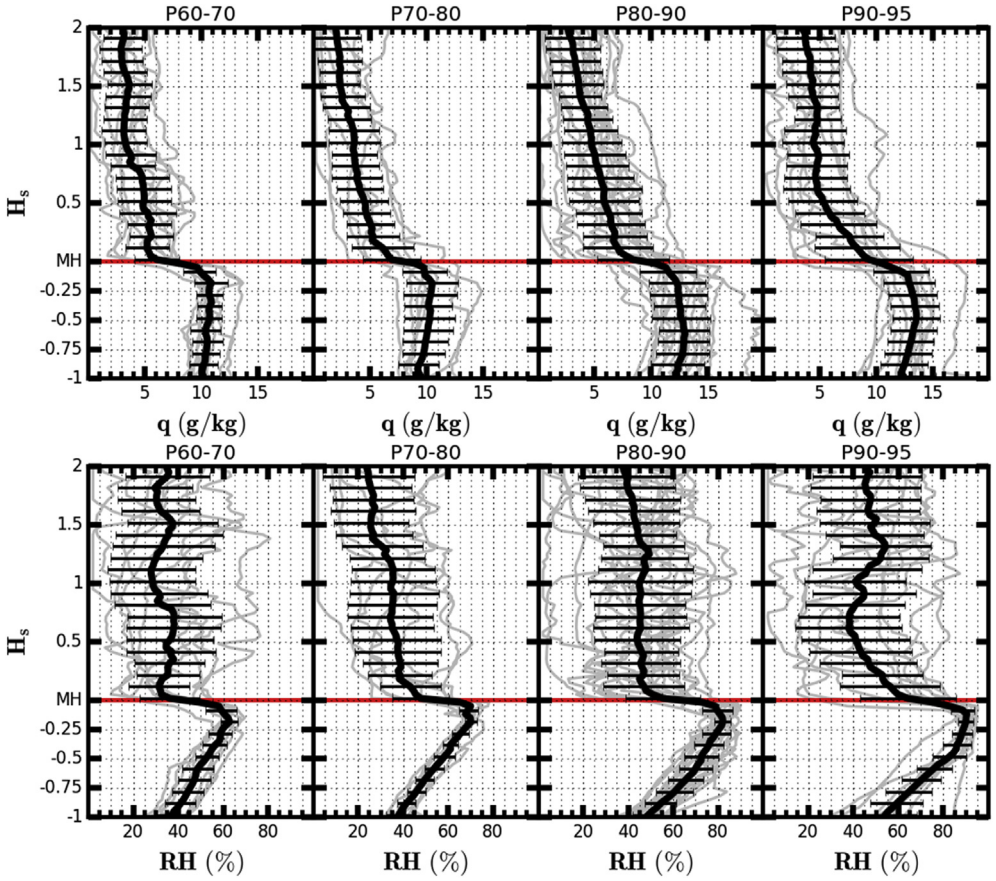

Fig. 4. The vertical structures of q and RH correspond to four groups of profiles from left to right. Within each group, the RH shows similar patterns within the mixed layer and significant differences in the free troposphere.

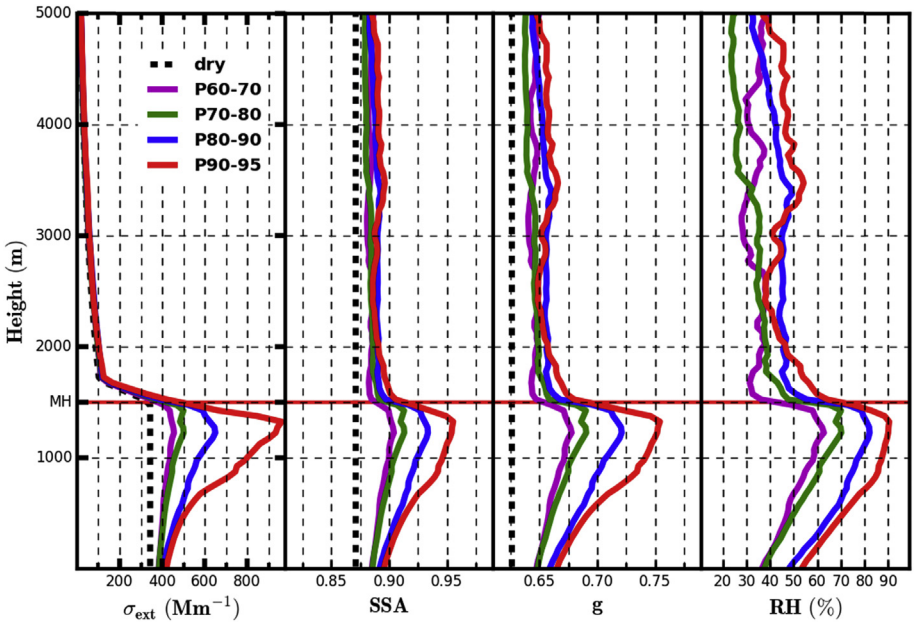

Fig. 5. The vertical structures of σ_{ext}, SSA and g at 550 nm under dry conditions and different RH profiles. These results demonstrate that the vertical variations in ambient aerosol optical properties are markedly different from those of dry aerosols and are highly dependent on the RH profiles.

significantly impacts the aerosol optical properties. These results indicate that RH profiles play an important role in the vertical structures of aerosol optical properties, particularly in very humid profiles, which are prevalent during the summer on the NCP.

AOD is widely used in current observation-based methods for estimating DARE (Myhre, 2009). When considering climate, it is important to quantitatively evaluate the impacts of RH profiles on AODs, which are rarely investigated. The previously mentioned P60–70, P70–80, P80–90 and P90–95, with MHs ranging from 700 m to 2000 m, were used to calculate the AOD according to the methods and assumptions introduced in Sect. 2.2. The corresponding results are shown in Fig. 6 and demonstrate that the ambient AOD is largely enhanced by ambient RH, with AOD increases of 17.8% (±0.8%), 21.8% (±1.4%), 39.4% (±2.7%) and 63.8% (±4.9%) due to aerosol water uptake under P60–70, P70–80, P80–90 and P90–95 conditions, respectively (also shown in Table 1). This result indicates that aerosol hygroscopic growth exerts a non-negligible influence on ambient AOD. The average AODs for P60–70, P70–80, P80–90 and P90–95 are 0.81, 0.84, 0.96 and 1.13, respectively. They are close to the average AOD values (0.9–1.3 for months from June to September) at Beijing (Xia et al., 2007) which are measured by ground-based sunphotometers from Aerosol Robotic Network (AERONET) (Holben et al., 2006). Moreover, for highly humid profiles that are prevalent during the summer on the NCP, RH is very important for determining ambient AOD. The differences between ambient and dry conditions slightly increase as the MH increases and the standard deviation of this difference is small for the same type of RH profile. Thus, the MRH is more important than the MH for determining the influences of aerosol hygroscopic growth on ambient AOD.

The column-averaged SSA and g retrieved from ground-based sunphotometers in the Aerosol Robotic Network (AERONET) and other platforms are widely used in measurement-based methods for estimating the DARE (Arola et al., 2013; Kassianov et al., 2013; Myhre, 2009). Therefore, the influences of different RH profiles on column-averaged SSA and g are also investigated. The average values of column-averaged SSA/g at 550 nm for P60–70, P70–80, P80–90, and P90–95 are 0.891/0.658, 0.895/0.663, 0.909/0.684 and

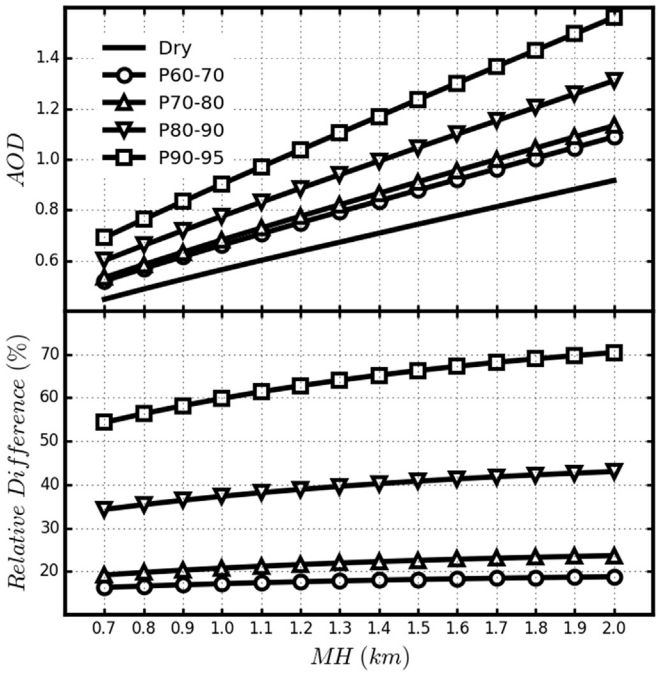

Fig. 6. The variations in the AOD at 550 nm under dry and different ambient RH conditions with different MH values and the relative differences between the AODs associated with different RH profiles compared to the AODs of dry-state aerosols.

Table 1
Relative increases of AOD and absolute increases of SSA and g due to aerosol hygroscopic growth: mean ± standard deviation.

	AOD (%)	SSA	g
P60–70	17.8 ± 0.8	0.021 ± 0.001	0.032 ± 0.001
P70–80	21.8 ± 1.4	0.024 ± 0.001	0.038 ± 0.002
P80–90	39.4 ± 2.7	0.038 ± 0.002	0.059 ± 0.003
P90–95	63.8 ± 4.9	0.052 ± 0.002	0.079 ± 0.004

Table 2
Cases for quantitatively understanding the influence of RH profiles on DARE estimations. In this table, 'dry'/'ambient' indicates that the aerosol optical properties obtained under dry/ambient conditions were used, and 'surface' indicates that the surface ambient value was used for the vertical profile.

	Case 1	Case 2	Case 3	Case 4	Case 5
σ_{ext}	Ambient	Dry	Ambient	Ambient	Ambient
SSA	Ambient	Dry	Dry	Ambient	Surface
g	Ambient	Dry	Dry	Dry	Surface

0.923/0.705, respectively. They are also close to the average values of SSA and g measured at Beijing from June to September which are retrieved from AERONET measurements (Xia et al., 2007). The average increments of column-averaged SSA/g at 550 nm due to aerosol hygroscopic growth for P60–70, P70–80, P80–90, and P90–95 are 0.021/0.032, 0.024/0.038, 0.038/0.059, and 0.052/0.079, respectively (averages and standard deviations are also shown in Table 1). These results demonstrate that aerosol hygroscopic growth has significant influences on column-averaged SSA and g, especially for highly humid RH profiles.

3.3. The influence of RH profiles on DARE estimations

As mentioned in the introduction, the influences of RH profiles on estimating DARE have rarely been investigated. Instead, it is generally assumed that the RH is constant across the aerosol layer. Four typical RH profiles representing humid and highly humid profiles are introduced in Sect. 3.1. The impacts of these RH profiles on the vertical structures of the aerosol optical properties are analyzed in Sect. 3.2. Overall, the results indicate that the uptake of water by aerosols may have non-negligible or significant impacts on the AOD, column-averaged SSA and g. Therefore, the five cases which are listed in Table 2 are designed to quantitatively understand the influences of different RH profiles on DARE estimates. Among these cases, Case 1 is designated as the standard case because all of the aerosol optical properties in this case are calculated at ambient RH conditions. By using the "dry" aerosol state, i.e., ignoring the dependence of RH on the aerosol optical properties, Case 2 is designed to show the fractional contribution of aerosol hygroscopic growth on DARE. In Cases 3 and 4, we similarly calculated the effect of RH on AOD and SSA. Thus, by comparing the results of the four cases, the individual contributions of the RH dependence of AOD, SSA and g on DARE estimations can be separated. In addition, during field campaigns, the surface SSA and g under ambient or dry conditions and the ambient AOD are usually observed. Furthermore, measurements from such field campaigns are often used to estimate the regional DARE (Cheng et al., 2008; Titos et al., 2014; Wendisch et al., 2008). Therefore, Case 5 was designed and the results of Cases 3 and 5 can be used to analyze the influences of using surface SSA and g measurements on the estimates of DARE. The results of cases corresponding to highly humid profiles are shown in Fig. 7, and the relative differences between the results of Cases 2, 3 and 5 and the standard case are listed in Table 3. The average instantaneous DARE for Case 1 at the TOA for P60–70, P70–80, P80–90, and P90–95 are −17.1 W m^{-2}, −18.7 W m^{-2}, −23.7 W m^{-2} and −30.1W m^{-2}, respectively. They have the same magnitude with the daily average DARE results (range from −58.1

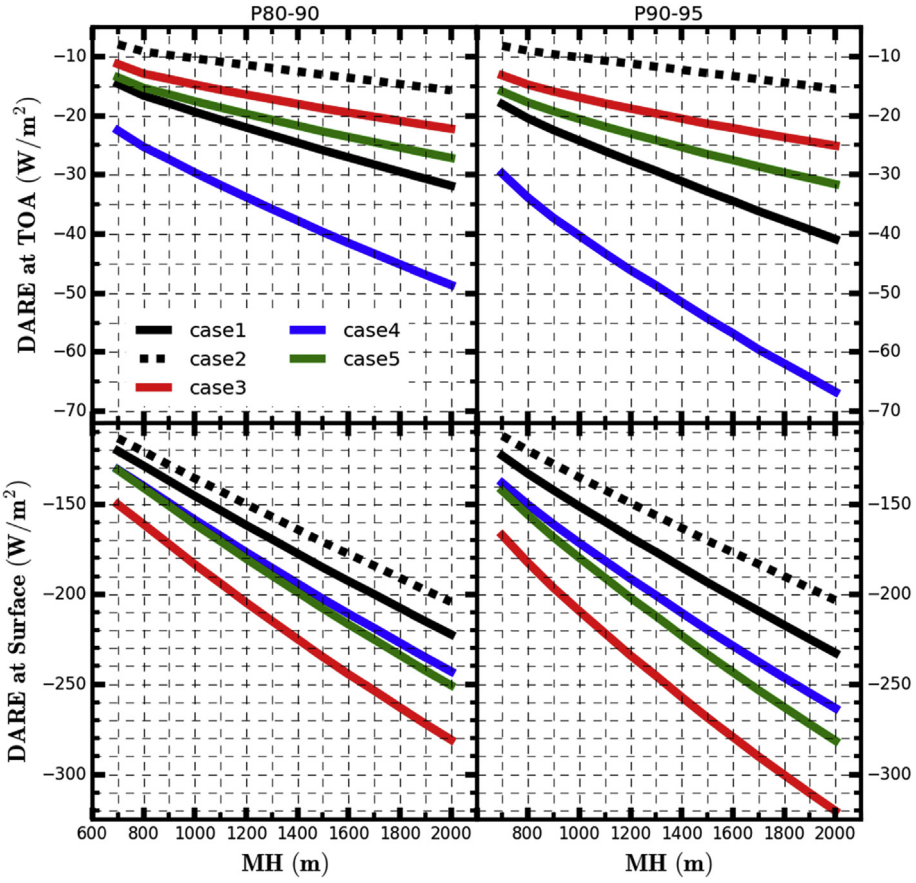

Fig. 7. The DARE at the TOA and the surface for the different cases shown in Table 1. These results demonstrate that estimates of DARE can be significantly biased if the RH dependence of SSA or g is not considered.

Table 3
Relative differences compared with Case 1: mean ± standard deviation (%).

	For the DARE at the TOA			For the DARE at the surface		
	Case 2	Case 3	Case 5	Case 2	Case 3	Case 5
P60–70	−31.3 ± 0.6	−17.1 ± 1.0	−3.3 ± 0.9	−3.3 ± 0.2	13.0 ± 0.2	4.1 ± 0.5
P70–80	−35.6 ± 1.6	−19.6 ± 1.8	−6.0 ± 1.7	−4.2 ± 0.4	15.6 ± 0.5	6.3 ± 0.8
P80–90	−48.4 ± 1.8	−26.3 ± 2.6	−11.3 ± 2.3	−7.7 ± 0.7	26.3 ± 0.6	11.5 ± 1.2
P90–95	−59.7 ± 2.3	−33.3 ± 3.7	−17.8 ± 3.3	−11.4 ± 1.1	38.2 ± 0.8	19.6 ± 1.5

to 0.1 W m^{-2}) estimated from AERONET measurements at Beijing (Xia et al., 2007) and daily average direct aerosol radiative forcing results (less than −10 W m^{-2}) at the NCP which are estimated with global chemical transport models (Ma et al., 2012b).

The results shown in Fig. 7 reveal that DARE at the TOA and surface are both enhanced by aerosol hygroscopic growth, especially the DARE at the TOA. For P90–95, the relative differences between the results from Cases 2 and 1 listed in Table 3 demonstrate that the fractional contribution to the instantaneous DARE at the local time of 13:30 and at the TOA due to aerosol hygroscopic growth can exceed 50%. Additionally, the fractional contribution to the DARE at the surface is relatively smaller. To better understand the different influences of aerosol hygroscopic growth on the DARE estimates at the TOA and the surface, the separate effects of the dependencies of the AOD, SSA and g on RH are shown in Fig. 7. The differences between the results in Cases 2 and 3 demonstrate that if the RH dependence of the AOD is considered, the DARE at both the TOA and the surface will be more negative, particularly for DARE at the surface. If the RH dependence on SSA is additionally considered, which corresponds to Case 4, the DAREs at the TOA and surface behave differently in comparison to Case 3. The DARE at the TOA is strongly affected and is more negative than results of Case 3. However, for DARE at the surface, which is also significantly modified but less negative than results of Case 3. This difference occurs because higher SSAs result in less absorption of incoming solar radiation by atmospheric aerosols, which allows more solar radiation to reach the ground. In contrast with Case 4, the RH dependence of g is also considered in Case 1, and the differences between the results demonstrate that the increasing g due to aerosol water uptake results in less negative DAREs at both the TOA and the surface because higher g values result in more forward scattering of solar radiation and the absorption of more solar radiation by atmospheric aerosols. In addition, more solar radiation will reach the ground and be absorbed by the ground surface. Overall, for DARE at the TOA, increases in the AOD and SSA due to aerosol water uptake will amplify the cooling effects induced by atmospheric aerosols, however, the RH dependence of g substantially compensates for these cooling effects. For DARE at the surface, the amplified cooling effects due to increases in AOD associated with aerosol water uptake are significantly offset by the RH dependency effects of SSA and g. The results of Cases 1 to 4 demonstrate that the RH dependencies of AOD, SSA and g all play significant roles in estimating the DARE and must be considered together when estimating the influences of RH on the DARE at the TOA and the surface. Large biases will occur when estimating the DARE if the RH dependence of SSA or g is not considered. Moreover, from results of Table 3, it can be seen that the standard deviations of relative differences of cases are very small for the same RH type, such as P90–95, these standard deviations are calculated by changing MH from 700 m to 2000 m. Which means that if standardized RH profiles are the same, relative contribution of aerosol water uptake to DARE varies little under different MH conditions. However, relative contribution of aerosol water uptake to DARE for RH profiles with different MRH levels differ significantly. Thus, it is thought that MRH level is more important than the MH in determining the fractal contribution of DARE associated with aerosol water uptake.

In addition, the results of Case 3 demonstrate that the estimation of DARE at the TOA and the surface will be significantly biased when using the SSA and g of dry-state aerosols observed at the surface. The results of Case 5 demonstrate that, compared with Case 3, using the surface SSA and g measurements of ambient aerosols has less influence on estimating the DARE at the TOA and the surface. However, this influence is not negligible, especially for highly humid profiles. Therefore, if the ambient vertical structures of SSA and g or their column-averaged values are absent, the ambient values of SSA and g at surface should be used. However, caution should be exercised when using SSA and g values from surface measurements.

4. Conclusions

From the vertical profiles of the meteorological parameters observed using radiosonde in Beijing at the local time of 13:30 from July to September in 2008, the vertical characteristics of RH on the NCP are characterized. The profiles with MRHs greater than 80% represent 52% of all the profiles that have distinct mixed layers. Which demonstrates that high RH profiles are prevalent during the summer on the NCP. The RH profiles are further coupled with surface measurements of aerosol properties to study the influences of RH profiles on aerosol optical properties. The ambient vertical structures of σ_{ext}, SSA and g are remarkably different from those of dry aerosols and are highly dependent on RH profiles. Increases of the aerosol optical depth and column-averaged SSA and g due to aerosol water uptake can reach up to 64%, 0.052 and 0.079, respectively. These results demonstrate that aerosol hygroscopic growth has significant influences on aerosol optical properties and RH profiles play significant roles.

Several cases have been designed to quantitatively estimate the influences of different levels of RH profiles on DARE estimates. The fractional contribution to the instantaneous DARE at the TOA due to aerosol hygroscopic growth reaches 60% in high RH profiles. Individual effects of the RH dependence of AOD, SSA and g on DARE are also studied. The calculated results demonstrate that DARE estimates can be significantly biased if the RH dependence of SSA or g is not considered. The results of designed cases also demonstrate that large biases occur if surface SSA and g are used to estimate the DARE at the TOA and surface, particularly for highly humid profiles. The ambient values of SSA and g at the surface, when used together, are better than the SSA and g values obtained from dry aerosols for estimating the DARE at the TOA and the surface. Thus, we suggest that the ambient values of SSA and g at the surface should be used rather than the values of SSA and g obtained from dry aerosols when estimating the DARE in the absence of their vertical profiles or column-averaged values.

Acknowledgments

We acknowledge the free MODIS surface albedo product, which was used in this study. This work is supported by the National

Natural Science Foundation of China (41590872, 41375134) and the Beijing Natural Science Foundation (8131003). The data used are listed in the references, tables and a repository at http://pan.baidu.com/s/1qXpj52s.

References

Arola, A., Eck, T.F., Huttunen, J., Lehtinen, K.E.J., Lindfors, A.V., Myhre, G., Smirnov, A., Tripathi, S.N., Yu, H., 2013. Influence of observed diurnal cycles of aerosol optical depth on aerosol direct radiative effect. Atmos. Chem. Phys. 13, 7895–7901.

Bian, J.C., Chen, H.B., Vomel, H., Duan, Y.J., Xuan, Y.J., Lu, D.R., 2011. Intercomparison of humidity and temperature sensors: GTS1, vaisala RS80, and CFH. Adv. Atmos. Sci. 28, 139–146.

Bian, Y.X., Zhao, C.S., Ma, N., Chen, J., Xu, W.Y., 2014. A study of aerosol liquid water content based on hygroscopicity measurements at high relative humidity in the North China Plain. Atmos. Chem. Phys. 14, 6417–6426.

Birmili, W., Stratmann, F., Wiedensohler, A., 1999. Design of a DMA-based size spectrometer for a large particle size range and stable operation. J. Aerosol Sci. 30, 549–553.

Bohren, C.F., Huffman, D.R., 2008. Absorption and Scattering of Light by Small Particles. Wiley, New York, USA.

Boucher, O., Randall, D., Artaxo, P., Bretherton, C., Feingold, G., Forster, P., Kerminen, V.-M., Kondo, Y., Liao, H., Lohmann, U., Rasch, P., Satheesh, S.K., Sherwood, S., Stevens, B., Zhang, X.Y., 2013. Clouds and aerosols. In: Stocker, T.F., Qin, D., Plattner, G.-K., Tignor, M., Allen, S.K., Boschung, J., Nauels, A., Xia, Y., Bex, V., Midgley, P.M. (Eds.), Climate Change 2013: the Physical Science Basis. Contribution of Working Group I to the Fifth Assessment Report of the Intergovernmental Panel on Climate Change. Cambridge University Press, Cambridge, United Kingdom and New York, NY, USA, pp. 571–658.

Brock, C.A., Wagner, N.L., Anderson, B.E., Beyersdorf, A., Campuzano-Jost, P., Day, D.A., Diskin, G.S., Gordon, T.D., Jimenez, J.L., Lack, D.A., Liao, J., Markovic, M.Z., Middlebrook, A.M., Perring, A.E., Richardson, M.S., Schwarz, J.P., Welti, A., Ziemba, L.D., Murphy, D.M., 2016. Aerosol optical properties in the southeastern United States in summer – Part 2: sensitivity of aerosol optical depth to relative humidity and aerosol parameters. Atmos. Chem. Phys. 16, 5009–5019.

Chen, J., Zhao, C.S., Ma, N., Liu, P.F., Göbel, T., Hallbauer, E., Deng, Z.Z., Ran, L., Xu, W.Y., Liang, Z., Liu, H.J., Yan, P., Zhou, X.J., Wiedensohler, A., 2012. A parameterization of low visibilities for hazy days in the North China Plain. Atmos. Chem. Phys. 12, 4935–4950.

Cheng, Y., Wiedensohler, A., Eichler, H., Heintzenberg, J., Tesche, M., Ansmann, A., Wendisch, M., Su, H., Althausen, D., Herrmann, H., 2008. Relative humidity dependence of aerosol optical properties and direct radiative forcing in the surface boundary layer at Xinken in Pearl River Delta of China: an observation based numerical study. Atmos. Environ. 42, 6373–6397.

Ferrero, L., Castelli, M., Ferrini, B.S., Moscatelli, M., Perrone, M.G., Sangiorgi, G., D'Angelo, L., Rovelli, G., Moroni, B., Scardazza, F., Močnik, G., Bolzacchini, E., Petitta, M., Cappelletti, D., 2014. Impact of black carbon aerosol over Italian basin valleys: high-resolution measurements along vertical profiles, radiative forcing and heating rate. Atmos. Chem. Phys. 14, 9641–9664.

Ferrero, L., Mocnik, G., Ferrini, B.S., Perrone, M.G., Sangiorgi, G., Bolzacchini, E., 2011. Vertical profiles of aerosol absorption coefficient from micro-Aethalometer data and Mie calculation over Milan. Sci. Total Environ. 409, 2824–2837.

Ferrero, L., Perrone, M.G., Petraccone, S., Sangiorgi, G., Ferrini, B.S., Lo Porto, C., Lazzati, Z., Cocchi, D., Bruno, F., Greco, F., Riccio, A., Bolzacchini, E., 2010. Vertically-resolved particle size distribution within and above the mixing layer over the Milan metropolitan area. Atmos. Chem. Phys. 10, 3915–3932.

Hignett, P., Taylor, J.P., Francis, P.N., Glew, M.D., 1999. Comparison of observed and modeled direct aerosol forcing during TARFOX. J. Geophys. Res. Atmos. 104, 2279–2287.

Holben, B., Eck, T., Slutsker, I., Smirnov, A., Sinyuk, A., Schafer, J., Giles, D., Dubovik, O., 2006. AERONET's version 2.0 quality assurance criteria, Remote Sensing of the Atmosphereand Clouds, Proc. SPIE 6408, 64080Q. http://dx.doi.org/10.1117/12.706524.

Im, J.S., Saxena, V.K., Wenny, B.N., 2001. An assessment of hygroscopic growth factors for aerosols in the surface boundary layer for computing direct radiative forcing. J. Geophys. Res. Atmos. 106, 20213–20224.

Kassianov, E., Barnard, J., Pekour, M., Berg, L.K., Michalsky, J., Lantz, K., Hodges, G., 2013. Do diurnal aerosol changes affect daily average radiative forcing? Geophys. Res. Lett. 40, 3265–3269.

Kuang, Y., Zhao, C.S., Tao, J.C., Ma, N., 2015. Diurnal variations of aerosol optical properties in the North China Plain and their influences on the estimates of direct aerosol radiative effect. Atmos. Chem. Phys. 15, 5761–5772.

Liu, P.F., Zhao, C.S., Zhang, Q., Deng, Z.Z., Huang, M.Y., Ma, X.C., Tie, X.X., 2009. Aircraft study of aerosol vertical distributions over Beijing and their optical properties. Tellus Ser. B-Chem. Phys. Meteorol. 61, 756–767.

Ma, N., Zhao, C.S., Müller, T., Cheng, Y.F., Liu, P.F., Deng, Z.Z., Xu, W.Y., Ran, L., Nekat, B., van Pinxteren, D., Gnauk, T., Müller, K., Herrmann, H., Yan, P., Zhou, X.J., Wiedensohler, A., 2012a. A new method to determine the mixing state of light absorbing carbonaceous using the measured aerosol optical properties and number size distributions. Atmos. Chem. Phys. 12, 2381–2397.

Ma, X., Yu, F., Luo, G., 2012b. Aerosol direct radiative forcing based on GEOS-Chem-APM and uncertainties. Atmos. Chem. Phys. 12, 5563–5581.

McMeeking, G.R., Morgan, W.T., Flynn, M., Highwood, E.J., Turnbull, K., Haywood, J., Coe, H., 2011. Black carbon aerosol mixing state, organic aerosols and aerosol optical properties over the United Kingdom. Atmos. Chem. Phys. 11, 9037–9052.

McMurry, P.H., 2000. A review of atmospheric aerosol measurements. Atmos. Environ. 34, 1959–1999.

Moteki, N., Kondo, Y., Miyazaki, Y., Takegawa, N., Komazaki, Y., Kurata, G., Shirai, T., Blake, D.R., Miyakawa, T., Koike, M., 2007. Evolution of mixing state of black carbon particles: aircraft measurements over the western Pacific in March 2004. Geophys. Res. Lett. 34.

Myhre, G., 2009. Consistency between satellite-derived and modeled estimates of the direct aerosol effect. Science 325, 187–190.

Petters, M.D., Kreidenweis, S.M., 2007. A single parameter representation of hygroscopic growth and cloud condensation nucleus activity. Atmos. Chem. Phys. 7, 1961–1971.

Ran, L., Deng, Z., Xu, X., Yan, P., Lin, W., Wang, Y., Tian, P., Wang, P., Pan, W., Lu, D., 2016. Vertical profiles of black carbon measured by a micro-aethalometer in summer in the North China Plain. Atmos. Chem. Phys. 16, 10441–10454.

Ricchiazzi, P., Yang, S., Gautier, C., Sowle, D., 1998. SBDART: a research and teaching software tool for plane-parallel radiative transfer in the Earth's atmosphere. Bull. Am. Meteorol. Soc. 79, 2101–2114.

Schafer, J.S., Eck, T.F., Holben, B.N., Thornhill, K.L., Anderson, B.E., Sinyuk, A., Giles, D.M., Winstead, E.L., Ziemba, L.D., Beyersdorf, A.J., Kenny, P.R., Smirnov, A., Slutsker, I., 2014. Intercomparison of aerosol single-scattering albedo derived from AERONET surface radiometers and LARGE in situ aircraft profiles during the 2011 DRAGON-MD and DISCOVER-AQ experiments. J. Geophys. Res. Atmos. 119, 7439–7452.

Shinozuka, Y., Clarke, A.D., Howell, S.G., Kapustin, V.N., McNaughton, C.S., Zhou, J., Anderson, B.E., 2007. Aircraft profiles of aerosol microphysics and optical properties over North America: aerosol optical depth and its association with PM2.5 and water uptake. J. Geophys. Res. Atmos. 112.

Srivastava, S., Lal, S., Subrahamanyam, D.B., Gupta, S., Venkataramani, S., Rajesh, T.A., 2010. Seasonal variability in mixed layer height and its impact on trace gas distribution over a tropical urban site: Ahmedabad. Atmos. Res. 96, 79–87.

Tao, J.C., Zhao, C.S., Ma, N., Liu, P.F., 2014. The impact of aerosol hygroscopic growth on the single-scattering albedo and its application on the NO2 photolysis rate coefficient. Atmos. Chem. Phys. 14, 12055–12067.

Titos, G., Lyamani, H., Cazorla, A., Sorribas, M., Foyo-Moreno, I., Wiedensohler, A., Alados-Arboledas, L., 2014. Study of the relative humidity dependence of aerosol light-scattering in southern Spain. Tellus Ser. B-Chem. Phys. Meteorol. 66, 15.

Wendisch, M., Hellmuth, O., Ansmann, A., Heintzenberg, J., Engelmann, R., Althausen, D., Eichler, H., Müller, D., Hu, M., Zhang, Y., Mao, J., 2008. Radiative and dynamic effects of absorbing aerosol particles over the Pearl River Delta, China. Atmos. Environ. 42, 6405–6416.

Xia, X., Chen, H., Goloub, P., Zhang, W., Chatenet, B., Wang, P., 2007. A compilation of aerosol optical properties and calculation of direct radiative forcing over an urban region in northern China. J. Geophys. Res. Atmos. 112, D12203.

Xu, W.Y., Zhao, C.S., Ran, L., Deng, Z.Z., Liu, P.F., Ma, N., Lin, W.L., Xu, X.B., Yan, P., He, X., Yu, J., Liang, W.D., Chen, L.L., 2011. Characteristics of pollutants and their correlation to meteorological conditions at a suburban site in the North China Plain. Atmos. Chem. Phys. 11, 4353–4369.

Yoon, S.C., Kim, J., 2006. Influences of relative humidity on aerosol optical properties and aerosol radiative forcing during ACE-Asia. Atmos. Environ. 40, 4328–4338.

Zieger, P., Fierz-Schmidhauser, R., Weingartner, E., Baltensperger, U., 2013. Effects of relative humidity on aerosol light scattering: results from different European sites. Atmos. Chem. Phys. 13, 10609–10631.